Formation of Box Canyon, Idaho, by Megaflood: Implications for Seepage Erosion on Earth and Mars
Michael P. Lamb, *et al.*
Science **320**, 1067 (2008);
DOI: 10.1126/science.1156630

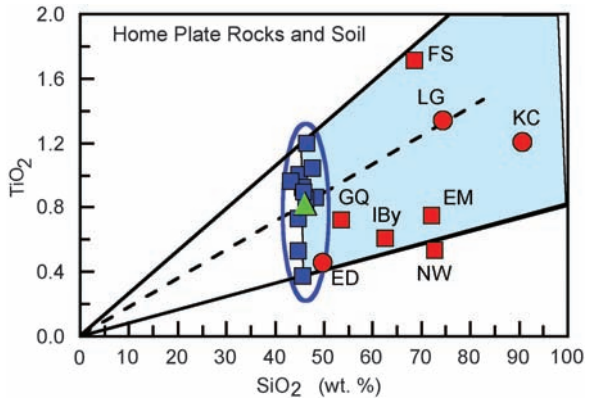

Fig. 5. Plot of titanium dioxide and silica contents for APXS measurements acquired since arriving at Home Plate and including observations from the Eastern Valley, Low Ridge, Mitcheltree Ridge, and the Tyrone areas. Red squares, silica-rich rocks; red circles, silica-rich soils; blue squares, basaltic rocks in the vicinity of Home Plate; and green triangle, typical local soil. The light blue region represents the compositions that can be obtained by acid-sulfate leaching of Home Plate rocks, assuming no variation in the TiO_2/SiO_2 ratio. KC, Kenosha Comets; LG, Lefty Ganote; FS, Fuzzy Smith; EM, Elizabeth Mahon; NW, Nancy Warren; ED, Eileen Dean; Iby, Innocent Bystander; and GQ, Good Question. The dashed line represents a typical evolutionary trend for leaching that preserves SiO_2 and TiO_2, and the blue oval indicates the range of basaltic rock compositions in the vicinity of Home Plate.

and dragged this nonrotating wheel along the surface, scraping paths through soils and crushing weak rocks.
17. J. W. Salisbury *et al.*, *Infrared (2.1-25 μm) Spectra of Minerals* (Johns Hopkins Univ. Press, Baltimore, 1991).
18. J. W. Salisbury *et al.*, *J. Geophys. Res.* **92**, 702 (1987).
19. J. F. Bell III *et al.*, *J. Geophys. Res.* **108**, 8063 (2003).
20. M. S. Rice *et al.*, Abstract #2138, presented at the 39th Annual Lunar and Planetary Science Conference, Houston, TX, 10 to 14 March 2008.
21. K. E. Herkenhoff *et al.*, *J. Geophys. Res.* **108**, 8065 (2003).
22. G. Klingelhöfer *et al.*, *J. Geophys. Res.* **108**, 8067 (2003).
23. Most of the rock and soil targets on the east side of Home Plate are named after players and teams from the All American Girls Professional Baseball League that operated from 1943 to 1954. The names are informal and not approved by the International Astronomical Union.
24. R. E. Arvidson *et al.*, *J. Geophys. Res.* **111**, E02S01 (2006).
25. P. M. Dove, J. D. Rimstidt, in *Silica: Physical Behavior, Geochemistry and Materials Applications*, P. J. Heaney, C. T. Prewitt, G. V. Gibbs, Eds. (Mineralogical Society of America, Washington, DC, vol. 29, 1994) pp. 259–308.
26. R. V. Morris *et al.*, *Lunar Planet. Sci.* **XXXI**, 2014 (2000).
27. K. A. Rodgers *et al.*, *Earth Sci. Rev.* **66**, 1 (2004).
28. K. A. Rodgers *et al.*, *Clay Miner.* **37**, 299 (2002).
29. H. D. Nam *et al.*, *Jpn. J. Appl. Phys.* **37**, 4603 (1998).
30. S. J. Kim, S. D. Park, Y. H. Jeong, *J. Am. Ceram. Soc.* **82**, 927 (1999).
31. W. P. Inskeep, T. R. McDermott, *Geothermal Biology and Geochemistry in Yellowstone National Park* (Thermal Biology Institute, Bozeman, MT, 2003).
32. M. R. Walter, D. J. Des Marais, *Icarus* **101**, 129 (1993).
33. W. N. Doemel, T. D. Brock, *Appl. Environ. Microbiol.* **34**, 433 (1977).
34. P. L. Siering *et al.*, *Geomicrobiol. J.* **23**, 129 (2006).
35. S. L. Cady, J. D. Farmer, in *Evolution of Hydrothermal Ecosystems on Earth (and Mars?)*, G. Bock, J. Goode, Eds. (J. Wiley and Sons, Chichester, UK, 1996), pp. 150–173.
36. S. Murchie *et al.*, *J. Geophys. Res.* **112**, E05S03 (2007).
37. R. E. Milliken *et al.*, Abstract P12A-02, presented at the American Geophysical Union Fall Meeting, San Francisco, CA, 10 to 14 December 2007.
38. This research was carried out for the Jet Propulsion Laboratory, California Institute of Technology, under a contract with NASA.

Supporting Online Material

www.sciencemag.org/cgi/content/full/320/5879/1063/DC1
Figs. S1 to S4
Table S1

18 January 2008; accepted 15 April 2008
10.1126/science.1155429

Formation of Box Canyon, Idaho, by Megaflood: Implications for Seepage Erosion on Earth and Mars

Michael P. Lamb,* William E. Dietrich, Sarah M. Aciego, Donald J. DePaolo, Michael Manga

Amphitheater-headed canyons have been used as diagnostic indicators of erosion by groundwater seepage, which has important implications for landscape evolution on Earth and astrobiology on Mars. Of perhaps any canyon studied, Box Canyon, Idaho, most strongly meets the proposed morphologic criteria for groundwater sapping because it is incised into a basaltic plain with no drainage network upstream, and approximately 10 cubic meters per second of seepage emanates from its vertical headwall. However, sediment transport constraints, ^4He and ^{14}C dates, plunge pools, and scoured rock indicate that a megaflood (greater than 220 cubic meters per second) carved the canyon about 45,000 years ago. These results add to a growing recognition of Quaternary catastrophic flooding in the American northwest, and may imply that similar features on Mars also formed by floods rather than seepage erosion.

A central thrust in geomorphology and planetary science is to link diagnostic landscape morphologies to formation processes. A prominent example is the formation of amphitheater-headed canyons, in which the stubby appearance of valley heads, steep headwalls, and little landscape dissection upstream have long been interpreted to result from seepage erosion or groundwater sapping on Earth (*1*–*4*), Mars (*5*, *6*), and now Titan (*7*). Theory (*8*), experiments (*9*), and field studies (*10*) have validated this hypothesis in unconsolidated sand, showing that valley heads are undermined and propagate upstream from seepage-induced erosion. This means that valleys can grow without precipitation-fed overland flow, which has profound implications for landscape evolution on Earth and the hydrologic cycle and habitability of Mars.

Despite widespread acceptance of the seepage-erosion hypothesis and its validation in sand, we lack an unambiguous example of an amphitheater-headed canyon formed by seepage erosion in bedrock because of overlapping features generated by rainfall runoff at most sites on Earth (*11*). Even the amphitheater-headed valleys of the Colorado Plateau and Hawaii, which are most often cited as classic examples of groundwater sapping in bedrock (*2*, *3*), have been in question because of evidence for flash floods and plunge-pool erosion (*11*–*13*). To better evaluate the seepage-erosion hypothesis, we set out to study the erosion and transport processes within a bedrock canyon, Box Canyon, Idaho, USA, which has a steep amphitheater-shaped headwall, contains the 11th-largest spring in the United States, and lacks the landscape dissection and rainfall runoff upstream of its headwall that has made other sites controversial (Fig. 1A). Moreover, Box Canyon exhibits remarkable similarity in morphology and possibly lithology (basalt) with many Martian canyons (Fig. 1B) that have been attributed to seepage erosion (*5*, *6*).

Box Canyon is located within the Snake River Plain, a broad and relatively flat basin in southern Idaho filled by sediments and volcanic flows that erupted over the course of ~15 million to 2 thousand years ago (ka) (*14*). Several tributaries of the Snake River Canyon appear as stubby valleys that end abruptly in amphitheater heads, including Malad Gorge, Blind Canyon, and Box Canyon (Fig. 2), all of which have been attributed to seepage erosion (*1*, *4*). Box Canyon is cut into the Sand Springs Basalt [also named the Basalt of Rocky Butte (*15*); see supporting online material (SOM) text] with an Ar-Ar eruption age of 95 ± 10 ka (*16*) and U-Th/He eruption ages that range from 86 +12 ka to 130 ± 12 ka (*17*), and this basalt filled an ancestral canyon of the Snake River (*18*).

Department of Earth and Planetary Science, University of California, Berkeley, CA 94720–4768, USA.

*To whom correspondence should be addressed. E-mail: mpl@berkeley.edu

The permeable lava beds of the Snake River Plain form an extensive aquifer, with recharge entering in the east [for example, Big Lost River sinks (Fig. 2)] and groundwater flowing westward. Large springs emanate from the east wall of the Snake River Canyon between Box Canyon and Malad Gorge, where the river jogs north, perpendicular to the regional topographic slope and the groundwater flow direction. These springs have a cumulative discharge of ~170 m^3/s, and one of the largest [~10 m^3/s (fig. S6)] emanates from the head of Box Canyon, creating Box Canyon Creek (*19*).

Box Canyon is sinuous (Fig. 3A), and the longitudinal profile is approximately 2.68 km in length and has an average channel-bed slope of 2.18% (Fig. 3B and fig. S3). The canyon is ~35 m deep and 120 m wide at its head and about twice as deep and wide at its mouth. The columnar basalt walls of the canyon have collapsed, creating steep (~20° to 35°) talus slopes, many of which abut Box Canyon Creek. Talus accumulation lessens upstream and is absent at the canyon head (Fig. 4A). Several terracelike platforms are elevated 2 to 7 m above the current stream level and separate the steep talus slopes from the creek (Fig. 3 and fig. S3). These contain large boulders (>1 m), and some appear to be imbricated in the downstream direction, indicating past fluvial transport.

Although the lack of talus at the canyon head has been taken as evidence of continued dissolution (*4*), the bedrock composing the headwall and surrounding talus are blocky and hard and show no visual evidence for enhanced weathering. Water samples from Box Canyon Creek and neighboring wells have silica concentrations of 32 to 35 mg/l, which bracket the saturation value (see SOM text and fig. S6), suggesting that the groundwater is in equilibrium with the basaltic aquifer and that substantial dissolution is not occurring at Box Canyon spring.

Despite no modern overland flow contribution to Box Canyon Creek, three features at the canyon head indicate that surface water once flowed into the canyon. First, three concentric semicircles of boulders within the canyon head appear to be waterfall plunge pools with ~2 m of relief (Fig. 4A). Second, a small notch (~300 m^3) in the center of the headwall rim (Fig. 4A) has linear flutelike abrasion marks, millimeters in width and several centimeters long, that follow the local curvature of the notch, indicating past overspill. The scours appear as divots on the inferred upstream end that gradually fan outward and diminish in relief downstream (Fig. 4B). Third, this scoured rock extends at least 1 km upstream of the canyon head and delineates flow toward the canyon (Fig. 3). The scoured path cannot be followed further upstream because it is covered by loess, deposited from ~40 to 10 ka (*20*).

The basalt in Box Canyon breaks down into large boulders (~1 m) that, without dissolution, must be transported downstream to allow canyon growth. Despite the great discharge of the spring, no measurable amount of sediment is currently transported. A minimum estimate of flow needed to carve the canyon can be found by calculating the discharge necessary to initiate sediment transport on the creek bed. We measured channel cross sections (fig. S4), longitudinal channel-bed profiles (Fig. 3 and fig. S3), and grain-diameter distributions (fig. S2) [diameter (D_{84}) = 0.6 m,

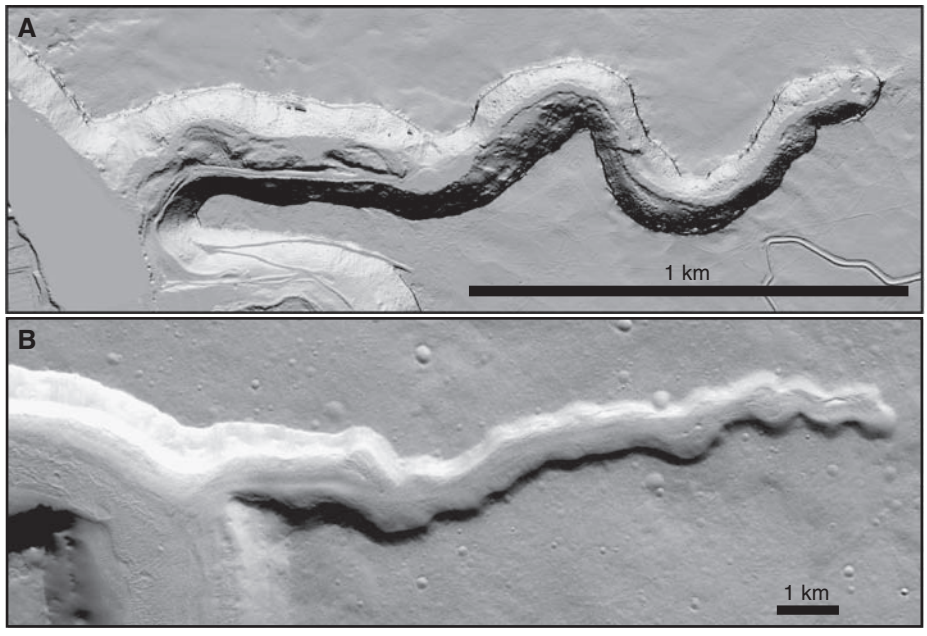

Fig. 1. (**A**) Shaded relief map of Box Canyon, Idaho. Airborne laser-swath mapping data were collected by the National Center for Airborne Laser Mapping. The data have been filtered to remove vegetation that exists along the creek banks. This is a Universal Transverse Mercator (UTM) zone 11 projection, North American Datum of 1983 (NAD83) datum, at 1 m resolution. (**B**) Thermal Emission Imaging System (*32*) infrared daytime image of Mamers Vallis, Mars, image V19470014, at 19 m resolution.

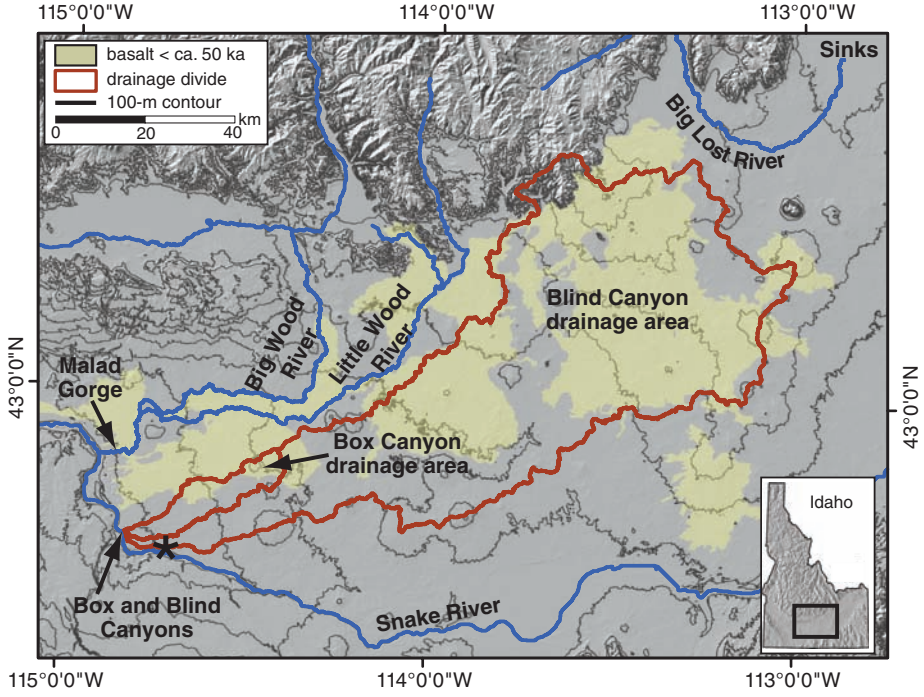

Fig. 2. Topographic map of the eastern Snake River Plain, the location of which is shown on the inset map of Idaho. The drainage areas feeding Box Canyon (228 km^2) and Blind Canyon (4713 km^2) are outlined, following the path of steepest descent. The yellow-shaded regions mark the locations of volcanism younger than ~50 ka (*15*). The thin black lines are 100-m topographic contours. Topographic data are from the U.S. Geological Survey. This is a UTM zone 11 projection, NAD83 datum, at 25 m resolution.

D_{50} = 0.29 m, and D_{16} = 0.13 m; the subscripts denote the percentage of grains that are finer] at a relatively straight 125-m reach within the canyon (Fig. 3A). A critical Shields stress formula for incipient motion (*21*) combined with our measured channel cross section (XS2 in Fig. 3A and fig. S4), local average bed slope (S = 1.85%; Fig. 3B and fig. S3), and a flow-resistance equation (*22*) determined that a flow discharge $Q > 220$ m^3/s (corresponding to an average flow depth $h > 1.7$ m) would be necessary to move the sediment bed and continue canyon erosion (*23*). This is a factor of 22 greater than the modern spring discharge ($Q \sim 10$ m^3/s).

The scoured-rock upslope of the canyon head occurs within a broad channel-like depression ~250 m wide and 3 m deep (XS1 in Fig. 3A and fig. S4). The scours extend over the southern bank of XS1, indicating that flow was deeper than and only partially bounded by this channel. A discharge estimate can be made for the flood event that spilled over the canyon rim by assuming that the flow was contained within this channel. Using the measured cross-sectional area at the threshold of overspill at XS1 (475 m^2), the regional bedrock slope parallel to scour marks (S = 0.74%), a flow-resistance formula (*22*), and a wide range in of bed-roughness length scales $0.1 \leq k_S \leq 1$ m (because this is the least-constrained parameter), we calculated a minimum flow discharge ranging from 800 to 2800 m^3/s (*23*). This would have filled the canyon to a depth of 3.7 to 5.8 m within our measurement reach (fig. S4), and, unlike seepage, would have exceeded the competency threshold to transport the bouldery bed. These estimated discharges are large, but smaller than the peak discharge of other catastrophic floods in the region [for example, the Bonneville flood, 10^6 m^3/s (*24*), and the Big Lost River Flood, 6×10^4 m^3/s (*25*)].

The vertical profile of the headwall suggests that it migrated upstream as a knickpoint, and the near-vertical joints inherent to flood basalt probably promoted toppling of basalt columns. The lack of gravel upstream of the canyon head also limited abrasion of the canyon rim. If sediment transport was the rate-limiting step for canyon erosion, a duration of flow needed to carve the canyon can be estimated by dividing the total volume of the canyon (~1.53×10^7 m^3) by a volumetric transport rate of sediment (*26*) for our estimates of flood discharge (800 to 2800 m^3/s). This suggests that flow was sustained for 35 to 160 days to transport the required load out of the canyon (*23*), which is similar to the estimated duration of the Bonneville flood [~100 days (*24*)]. Excavation of Box Canyon could have taken less time, however, because the flood was only partially contained within the channel at XS1.

We collected four samples, distributed in the streamwise direction within the canyon (Fig. 3), for ^{3}He cosmogenic-exposure–age dating to further constrain the history of the canyon. We sampled scoured bedrock that was exposed at the canyon-head rim [location 4 (Fig. 4B)], and three large boulders that, from their size and separation from the active talus slopes, appeared to be relatively stable (fig. S1B). Active talus production from canyon walls, as well as weathering, means that the ages for these boulder surfaces provide minimum ages of the canyon.

Of the boulders sampled, only location 2 was on a terrace among other large imbricated boulders, potentially indicating past fluvial transport (Fig. 3 and fig. S1B). This sample yielded an exposure age of 48 ± 3 ka (1 σ error) and the other two boulders were nearly half as old

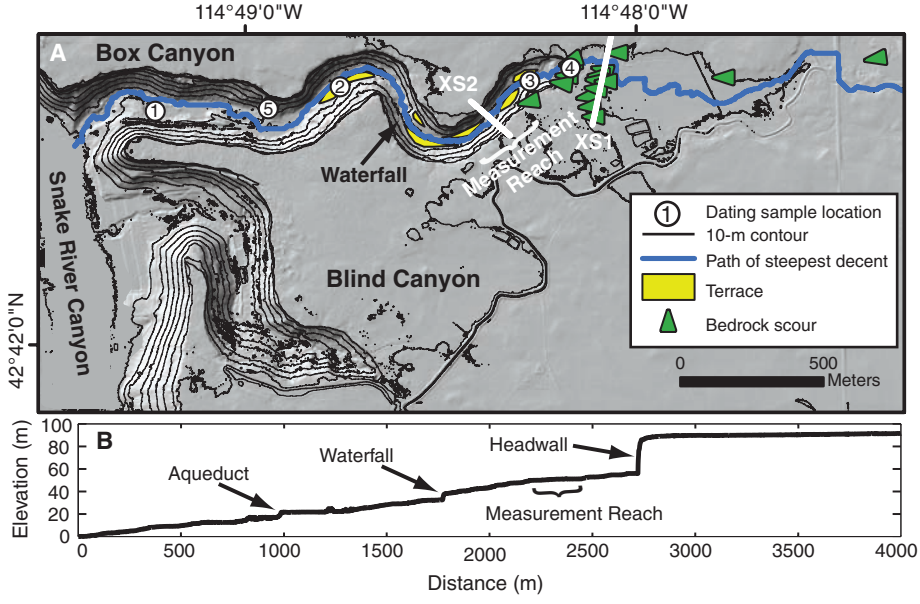

Fig. 3. (**A**) High-resolution topographic map of Box and Blind Canyons. The yellow-shaded regions mark potential fluvial terraces, which range from 2 to 7 m above the current stream level (fig. S3). Detailed measurements of flow depth, water surface slope, bed slope, channel width, and bed particle size were made within the region marked "measurement reach" (*23*). Discharge calculations were made using cross-sectional areas measured at XS1 and XS2 (fig. S4). Mapped scours on bedrock (Fig. 4B) are shown as green arrows. The white circles are sample locations used for dating. The thin black lines are 10-m topographic contours. The blue line is the calculated path of steepest descent, but does not indicate modern-day flow paths because no flow on record has spilled over the canyon headwall. See Fig. 1 for data source and projection. (**B**) Longitudinal profile of Box Canyon extracted from light detection and ranging data (Fig. 3A), following the path of steepest descent. Major breaks in slope correspond to the canyon headwall, waterfall, and a disturbed region near the canyon mouth caused by an aqueduct.

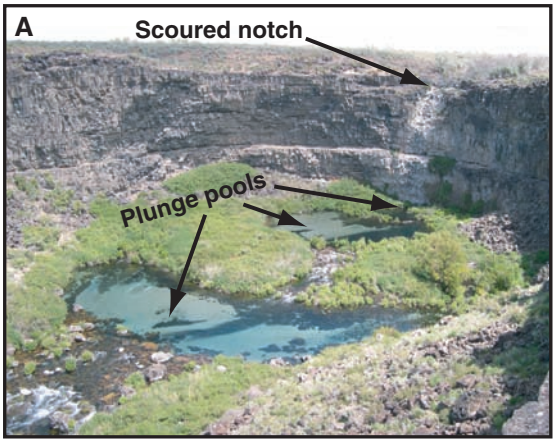

Fig. 4. (**A**) Photograph of the head of Box Canyon. The three concentric circles that lack boulders are interpreted to be plunge pools. The headwall relief is ~35 m. (**B**) Photograph of scours within the notch of the Box Canyon headwall. The pencil included for scale is ~14 cm long and points in the inferred flow direction.

(location 1, 21 ± 1 ka; location 3, 19 ± 3 ka) (*17*, *23*). The scoured notch (location 4) yielded the same age as the boulder at location 2, 45 ± 5 ka.

Another constraint on the age of the canyon comes from an ~20-cm-thick, finely laminated bed, containing clay, silt, and sand, that is exposed in a small road cut within the talus slope [location 5 (Fig. 3 and fig. S1C)]. Two shells found within the layer yielded ages of 22.4 ± 1 × 10^3 radiocarbon years before the present (*23*), which is equivalent to a calibrated age of ~26 ka (*27*).

Together, these observations, hydraulic calculations, and dates eliminate the seepage-erosion hypothesis for the formation of Box Canyon. Here, seepage is not substantially enhancing the weathering of the headwall, and contemporary seepage flow is deficient by a factor of ~22 to evacuate sediment from the canyon. Moreover, erosion of the canyon headwall ceased ~45 ka according to the age of the scoured-bedrock notch. The observations of scoured bedrock and plunge pools point toward a flood or floods able to transport boulders and carve the canyon in weeks or months, illustrating the power of rare catastrophic events in shaping landscape. This hypothesis is supported by the similarity in surface-exposure ages of the terrace-bound boulder at location 2 and the scoured notch. We interpret the younger boulders to have rolled to the canyon floor after the canyon was formed, which is consistent with the shell deposit sandwiched between several meters of talus (fig. S1C), indicating that canyon formation occurred well before 22 ka and wall collapse has been active since. Whereas a single flood event is the simplest interpretation, we cannot rule out multiple events occurring after 86 ± 12 ka [the eruption age of the basalt (*17*)], with the last event resetting the exposure ages to ~45 ka.

The dates indicate that the canyon is much older than the Bonneville flood that occurred within the Snake River Canyon ~14.5 ka. Given the drainage area of Box Canyon (228 km^2) and Blind Canyon (4713 km^2) (Fig. 2), and our flood-duration and discharge estimates, a sufficient meteorological flood would require more than 1.7 m of runoff lasting for several weeks or longer, which is highly unlikely because modern annual precipitation averages only 0.22 m over the eastern Snake River Plain, infiltration is extremely high, and conditions were probably drier ~45 ka (*28*). Potential diversions of the Snake River by lava flows also seem unlikely because the Snake River Canyon and the Box and Blind drainages are separated topographically, except for one location (marked with an asterisk on Fig. 2), and no volcanic dams with an age of ~45 ka have been discovered there.

The most likely source for the Box Canyon flood is the Little and Big Wood River drainage basins to the north or the Big Lost River drainage basin to the northeast (Fig. 2). Both drainages produced large-magnitude paleofloods that cut canyons in Quaternary basalt, scoured bedrock, and transported large (~1 m) boulders (*15*, *25*). For example, the paleomegaflood of the Big Lost River, which occurred sometime between ~19 ka and 95 ka (*29*), was probably an outburst from the Pleistocene Glacial-Lake East Fork and had a peak flow of 6 × 10^4 m^3/s (*25*). Such an event would have easily surpassed the drainage divide between Box Canyon and the Wood and Lost River drainages (Fig. 1). The divides themselves also have shifted since the formation of Box Canyon because of volcanism that postdates the Box Canyon flood (Fig. 2).

Our findings suggest that Box Canyon and other amphitheater-headed canyons carved into basalt by large floods [for example, Dry Falls, Washington, USA (*30*), and Ásbyrgi Canyon, Iceland (*31*)] might be better terrestrial analogs of Martian canyons in volcanic terrains than seepage channels in sand.

References and Notes

1. I. C. Russel, *U.S. Geol. Surv. Bull.* **199**, 192 (1902).
2. J. E. Laity, M. C. Malin, *Geol. Soc. Am. Bull.* **96**, 203 (1985).
3. R. C. Kochel, J. F. Piper, *J. Geophys. Res.* **91**, E175 (1986).
4. H. T. Stearns, *J. Geol.* **44**, 429 (1936).
5. M. C. Malin, M. H. Carr, *Nature* **397**, 589 (1999).
6. K. P. Harrison, R. E. Grimm, *J. Geophys. Res.* 10.1029/200JE002455 (2005).
7. M. G. Tomasko *et al.*, *Nature* **438**, 10.1038/nature04126 (2005).
8. T. Dunne, *Prog. Phys. Geogr.* **4**, 211 (1980).
9. A. D. Howard, C. F. McLane, *Water Resour. Res.* **24**, 1659 (1988).
10. S. A. Schumm, K. F. Boyd, C. G. Wolff, W. J. Spitz, *Geomorphology* **12**, 281 (1995).
11. M. P. Lamb *et al.*, *J. Geophys. Res.* **111**, 10.1029/2005JE002663 (2006).
12. M. P. Lamb, A. D. Howard, W. E. Dietrich, J. T. Perron, *Geol. Soc. Am. Bull.* **119**, 805 10.1130/B25986.1 (2007).
13. A. D. Howard, W. E. Dietrich, M. A. Seidl, *J. Geophys. Res.* **99**, 13971 (1994).
14. H. E. Malde, in *Quaternary Nonglacial Geology; Conterminous U.S.*, R. B. Morrison, ed. [Geological Society of America (GSA), Boulder, CO, 1991], vol. K-2.
15. J. D. Kauffman, K. L. Otherberg, V. S. Gillerman, D. L. Garwood, *Geologic Map of the Twin Falls 30 × 60 minute Quadrangle, Idaho* (Idaho Geological Survey, Moscow, ID, 2005).
16. L. Tauxe, C. Luskin, P. Selkin, P. Gans, A. Calvert, *Geochem. Geophys. Geosyst.* **5**, 10.1029/2003GC000661 (2004).
17. S. M. Aciego *et al.*, *Earth Planet. Sci. Lett.* **254**, 288 10.1016/j.epsl.2006.11.039 (2007).
18. H. E. Malde, *U.S. Geol. Surv. Prof. Pap.* **20**, 20 (1971).
19. U.S. Geological Survey: Box Canyon creek, gauge 13095500. This well log information can be found at http://waterdata.usgs.gov/awis.
20. S. L. Forman, R. P. Smith, W. R. Hackett, J. A. Tullis, P. A. McDaniel, *Quat. Res.* **40**, 30 (1993).
21. M. P. Lamb, W. E. Dietrich, J. Venditti, *J. Geophys. Res.*, doi:10.1029/2007JF000831 (2008).
22. J. C. Bathurst, *J. Hydrol. (Amst.)* **269**, 11 (2002).
23. Materials and methods are available as supporting material on *Science* Online
24. J. E. O'Connor, *Hydrology, Hydraulics and Geomorphology of the Bonneville Flood*, (GSA Special Paper 274, GSA, Boulder, CO, 1993), p. 90.
25. S. L. Rathburn, *Geomorphology* **8**, 305 (1993).
26. R. Fernandez Luque, R. van Beek, *J. Hydraul. Res.* **14**, 127 (1976).
27. P. J. Reimer *et al.*, *Radiocarbon* **46**, 1029 (2004).
28. D. B. Madsen *et al.*, *Palaeogeogr. Palaeoclimatol. Palaeoecol.* **167**, 243 (2001).
29. T. E. Cerling, R. J. Poreda, S. L. Rathburn, *Geology* **22**, 227 (1994).
30. J. H. Bretz, *J. Geol.* **31**, 617 (1923).
31. H. Tomasson, *Natturufraeoingurinn* **43**, 12 (1973).
32. P. R. Christensen *et al.*, *Space Sci. Rev.* **110**, 85 (2004).

33. Funding was provided by the NASA Astrobiology Institute and the National Center for Earth Surface Dynamics. We thank C. May, J. McKean, T. Perron, R. Thurow, and T. van Soest for field assistance.

Supporting Online Material

www.sciencemag.org/cgi/content/full/320/5879/1067/DC1
Materials and Methods
SOM Text
Figs. S1 to S6
Table S1

19 February 2008; accepted 21 April 2008
10.1126/science.1156630

Anticorrelated Seismic Velocity Anomalies from Post-Perovskite in the Lowermost Mantle

Alexander R. Hutko,[1]* Thorne Lay,[1]† Justin Revenaugh,[2] Edward J. Garnero[3]

Earth's lowermost mantle has thermal, chemical, and mineralogical complexities that require precise seismological characterization. Stacking, migration, and modeling of over 10,000 *P* and *S* waves that traverse the deep mantle under the Cocos plate resolve structures above the core-mantle boundary. A small −0.07 ± 0.15% decrease of *P* wave velocity (V_p) is accompanied by a 1.5 ± 0.5% increase in *S* wave velocity (V_s) near a depth of 2570 km. Bulk-sound velocity [$V_b = (V_p^2 - 4/3V_s^2)^{1/2}$] decreases by −1.0 ± 0.5% at this depth. Transition of the primary lower-mantle mineral, $(Mg_{1-x-y}\ Fe_xAl_y)(Si,Al)O_3$ perovskite, to denser post-perovskite is expected to have a negligible effect on the bulk modulus while increasing the shear modulus by ~6%, resulting in local anticorrelation of V_b and V_s anomalies; this behavior explains the data well.

Increasing pressure (*P*) and temperature (*T*) with depth in Earth causes minerals to undergo phase transitions to new crystalline structures accompanied by abrupt changes in density (ρ), isentropic bulk modulus (K_S), and shear modulus (*G*) that result in seismic *P* wave velocity $\{V_p = [(K_S + 4/3G)/\rho]^{1/2}\}$ and *S* wave velocity $[V_s = (G/\rho)^{1/2}]$ discontinuities. The pri-